Predictive Modelling and Simulation of Baseball Pitching by Optimizing Muscle Torque Generator Temporal Activation Patterns

Cedric E. Attias
Motion Research Group
Mechanical and Mechatronics Engineering, University of Waterloo
Waterloo, ON, Canada

***Abstract*—This paper outlines the modeling, simulation, and optimization of a simplified biomechanical model of the trunk and throwing arm during a fastball baseball pitch. The model relies on muscle torque generators (MTG) at the trunk, shoulder, elbow, and wrist joints to act as actuators which simulate muscle forces. The MTG actuation is governed by a piece-wise function, which contains variables for the activation and deactivation times of the torques. These times are optimized to produce the maximum pitching velocity in the direction of the batter, using both particle swarm and pattern search optimization techniques. The outputs of the optimization produce the optimized temporal joint firing variables for each degree of freedom (DOF) in the model, which are used as inputs into an optimized simulation. Comparisons between the optimized model's behaviour and measured biomechanical data from literature shows similarities in joint trajectories and positions, but are flawed due to model assumptions and differences in initial conditions.**

***Index Terms*—Baseball, Pitching, Biomechanics, Modelling, Simulation, Optimization**

I. Introduction

A. Problem Description and Background

In sports, obtaining a competitive edge over the competition is essential to producing the best possible outcomes. However, there is a trade-off between performance and injury that may put players at risk of missing prolonged periods of time. No athlete struggles with this balance more than a baseball pitcher. In 2018, 13% of MLB players and their minor league affiliates underwent elbow ligament reconstruction, for a total of 637 athletes, with pitchers occupying a large majority of the affected population [1],[2]. Additionally, from 2013-2018, pitchers missed over 14,000 regular season days costing teams $193.5 million on athletes who didn't participate [1],[2].

The repetitive overhead motion in baseball pitching places extreme loads and stresses on the musculoskeletal system, namely the shoulder and elbow [3]. Shoulder and elbow forces and torques have been studied thoroughly in baseball and are responsible for soft tissue microtrauma experienced at the extremes of the range of motion (ROM) during a pitch [3-11]. An understanding of pitching mechanics and their effect on the kinetic chain is essential to allowing the athlete to avoid injury [3]. The kinetic chain in pitching can be thought of as an interaction of body segments, in a sequential pattern from the ground up, and from more proximal segments to distal ones. The chain terminates at the end-effector, which is the ball-hand complex in this case [3]. Examining the kinetic chain during a pitch can also inform performance. Seamless sequencing of the kinetic chain can lead to an increase the velocity of the terminal segment, thus maximizing ball speed at release [4-11]. By maximizing ball speed, a pitcher can increase the likelihood of throwing a strike, since the increased ball speed may elude the batter more easily, improving the thrower's performance.

The arms kinetic chain sequencing is very much related to the activation and deactivation times of the muscles of the throwing arm, which is a crucial variable to address [11]. As stated by Alexander [11], there is an optimal pattern between activation of the proximal muscles and of the distal ones, which maximizes the speed at which a projectile can leave the hand. From a physiological perspective, if the delay between proximal and distal muscle activation is too fast, the throw may be completed sooner, and less time is available for contraction of the proximal muscle [11]. This may result in decreased torque generation or torque generation over a smaller ROM, ultimately reducing the work done by the muscles on the ball [11].

Evidently, there is a dire need for research in the area of pitching mechanics, which can be addressed through modelling, simulation, and optimization to avoid any unnecessary stresses that may be associated with experimentation on pitchers. As such, the aim of this report is to outline the process of developing a multi DOF, 3-dimensional (3D) model of a pitcher's throwing arm and trunk, which will serve as the foundation for a more complex, full-body model in the future. Cumulative muscle forces will be modelled as MTG, which actuate joint movements, where the actuator firing times will be optimized to maximize velocity of the end-segment towards the batter. It is important to note that this project will only be modelling and simulating the arm acceleration phase of the pitching movement, and not the entire pitch, for the sake of simplicity. The arm acceleration phase begins with front-foot contact with the ground, where the shoulder is maximally externally rotated, and ends when the ball is released.

B. Literature Review

There is an extensive number of publications discussing the biomechanics of baseball pitching, several of which have al-

ready been referenced [3-11]. The purposes of the studies vary, however, these papers are kinematic descriptive ones. This means that they measure and report the pitching kinematics, and draw conclusions from there. While these studies are useful, they do not offer much with respect to the goals of this study, besides for validation and comparison purposes.

Very few papers discuss the modelling, simulation, and optimization of baseball mechanics, which may be because of the degree of difficulty in such a problem. The studies that exist are either too vague in their description of the techniques employed, use outdated techniques, or are simply published too long ago to offer any sort of modern value. This does not imply that research of this nature does not exist, but it may mean that the private baseball organizations conducting such research may not be publishing their conclusions, as to not provide the opposition with the same competitive edge they gain from this work.

One such work published by Matsuo et al. in 2002 investigates the effects of shoulder abduction angle on ball velocity and on the injury-related joint kinetic variables [12]. Kinematic data was collected and used to simulate pitching motions by varying the shoulder abduction angle from the measured angle. Optimization was employed with the various simulation conditions to determine maximum pitching velocity at a given angle. They then use the optimized kinematics to evaluate injury potential. The article claims to employ optimization techniques but does not discuss the formulation or execution at all. It also used outdated data collection techniques and was published over 20 years ago.

Another paper by Fujii et al. published in 2002, created a model, and a simulation and optimization procedure were constructed to investigate the relationships between optimal movement and muscular strength for baseball pitching using torque generators [13]. They used the steepest descent method with a complex objective function to optimize the muscle activation of each torque generator. Although this article describes the optimization formulation and implementation in detail, the musculoskeletal modelling and simulation approaches are outdated, and the paper is over 20 years old.

It is also useful to evaluate similar work in other sports. Models such as the one created by McNally and McPhee [14], attempt to optimize a biomechanical model of a golf swing to maximize distance by designing a control system for MTG [14]. In this work, the torque timings for the golf swing were parameterized and resolved using optimization. This work was a major source of inspiration for this project, and many techniques used in the publication were applied to this project.

II. Modelling

A. MapleSim Modelling Implementation

The biomechanical model created consists of 4 rigid-body segments, being the combined trunk and pelvis, upper-arm, forearm, and hand/ball, which is shown in Figure 1. The trunk and pelvis are rigidly connected, fixed to the ground, and restricted from translating. The hand and ball are modelled to be rigid since contact modelling is beyond the project scope. The model was created in accordance with anthropometric measurements, which accurately describe the centre of mass (COM) position, lengths, masses, and moments of inertia (MOI) of all segments as shown in Table 1. The inertial parameters came from that of an average male (73 kg weight and 1.741 m height) as published by de Leva. [15]. The ball radius, mass, MOI and density were also found from literature, modelled as a solid sphere, and matches the properties of a regulation baseball [16].

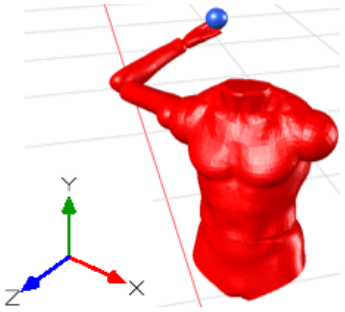

Fig. 1. 3D MapleSim biomechanical model. The model is oriented so that x-axis points anteriorly, y-axis points upwards and z-axis points to the right. The direction of the batter is the positive x-direction, as depicted by the red line.

The model was assembled in MapleSim (Maplesoft Inc., Waterloo, ON, Canada) and is a non-linear dynamic model with a total of 5 degrees of freedom. In the back-end of the software, highly complex differential equations govern the movement of the model. Each DOF represents a joint movement and is modelled as a single DOF hinge joint. Note that based on the local joint coordinate systems and the right-hand rule, movements are designated as positive or negative (Table 2). The included DOF are as follows and highlighted in Table 2: ***1)*** trunk medial/lateral axial rotation (MAR/LAR), ***2)*** shoulder horizontal flexion/extension (H. FLX/EXT), ***3)*** shoulder internal/external rotation (IR/ER), ***4)*** elbow flexion/extension (E. FLX/EXT), and ***5)*** wrist flexion/extension (W. FLX/EXT).

In general, each DOF was actuated by two MTG to enable motion in each direction. However, recall that only the arm acceleration phase is being modelled. This means that the model will move in one direction, and not all actuators are needed. The unnecessary actuators are set to zero since that movement does not occur during this pitching phase. More specifically, at no point does the shoulder require extension or external rotation and the trunk does not need lateral axial rotation, during the pitching phase being modelled. In summary there are a total of seven MTG actuating movement across five DOF, some of them being only in one direction. The model DOF and initial conditions are summarized in Table 2, while the activated movements are seen later Table 4. Note that the trunk is not a joint, but will be referred to as a joint when discussing its DOF. In reality, MAR/LAR movements come from a number of different joints, but are being lumped together and called the trunk for simplicity.

TABLE I
SEGMENT INERTIAL PROPERTIES [15,16]

Segment	Mass (kg)	Length (m)	MOI (kg m ^{2})
Hand	0.4526	0.193	0.0004
Forearm	1.1826	0.271	0.0052
Upper-Arm	1.9783	0.284	0.01
Trunk+Pelvis	32	0.38	0.44
Ball	0.145	0.0375 (radius)	0.000082

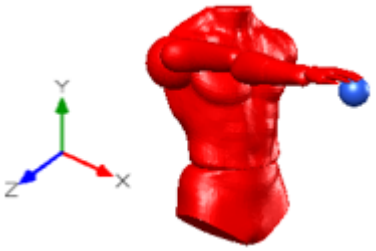

Fig. 2. Neutral position of the model. All angles taken are in reference to this position. Based on the definition, the trunk rotation, shoulder flexion and elbow flexion DOF is about the y-axis, while shoulder rotation is about the x-axis and wrist flexion is about the z-axis.

TABLE II
MOVEMENT OF THE MODEL (TOP) AND INITIAL CONDITIONS (BOTTOM) [8],[17,18]

Joint	DOF)	Movements
Wrist	1 (z-axis)	FLX(-)/EXT(+)
Elbow	1 (y-axis)	FLX(+)/EXT(-)
Shoulder	2 (y,x-axis)	H. FLX(+)/EXT(-), IR(-)/ER(+)
Trunk	1 (y-axis)	MAR(+)/LAR(-)

Joint	θ_0 (From Neutral as in Fig. 2)	V_0
Wrist	0°	0°/s
Elbow	90° FLX	1212°/s EXT
Shoulder	120° EXT, 160° ER	205 °/s FLX, 0°/s
Trunk	35° LAR	489°/s MAR

The initial conditions for the model are values from literature that were extracted from experimentation which examined the kinematics of the arm acceleration phase of the pitch and are summarized in Table 2 [8],[17,18]. Note that at the starting position, the shoulder is maximally externally rotated and extended, and the trunk is maximally laterally rotated, which is why the MTG for those movements are set to zero. Moreover, the shoulder begins at 30° in extension from the positive z-axis, externally rotated 160° from the positive x-axis, the elbow is flexed and shoulder abducted to 90°, the wrist is neutral and the trunk is laterally rotated -35° from the positive y-axis [8],[17]. The positional initial conditions can be seen in Figure 1. When the model was being simulated, there seemed to be a lag between the MTG activation and the movement. This was because originally, the model did not have any initial velocity. Since the arm acceleration phase occurs in the middle portion of the whole pitching motion, there should be an initial velocity at the begging of arm acceleration. These values were identified from literature and included in the model to compensate for the lag as seen in Table 2 [18].

B. Muscle and Torque Modelling

With the model created, it is essential to encapsulate the behaviour of the joint actuators. A similar approach was taken as in [14], and was implemented for each MTG. The active MTG torques (T_{active}), can be formulated using a piecewise function that varies with the shortening rate of the joint as follows:

$$T_{\text{active}} = \begin{cases} T_{\text{isometric}}\left(\frac{\omega_{\max}-\omega}{\omega_{\max}+r\omega}\right) & \omega \geqslant 0 \\ T_{\text{isometric}}\left(\frac{(1-T_r)\omega_{\max}+S\omega T_r(r+1)}{(1-T_r)\omega_{\max}-S\omega(r+1)}\right) & \omega < 0 \\ 0 & \omega > \omega_{\max} \end{cases}$$

where ω is the joint's current shortening rate, $\omega_{\max}$ is joint's maximum rate of shortening (60 rad/s for all DOF except the trunk is 30 rad/s in this model), r is the shape factor (1.5 for this model), T_r is the ratio between the maximum eccentric and isometric force (1.5 in this model), and S is the ratio between the eccentric and concentric derivatives of force with respect to the velocity at maximum isometric force (2 used in this model). The isometric torque component is written as follows:

$$T_{\text{isometric}} = T_{\max}(1 - e^{\frac{-t_{\text{on}}}{t_{\text{act}}}})^n - T_{\max}(1 - e^{\frac{-t_{\text{off}}}{t_{\text{deact}}}})^n$$

Where $T_{\max}$ is the maximum isometric torque for the joint (450 Nm, 160 Nm, 90 Nm, and 60 Nm used for the trunk, shoulder, elbow and wrist joint, respectively), $t_{\text{act}}$and $t_{\text{deact}}$are the respective activation and deactivation time constants (where activation is 0.00000001s and deactivation is 0.00000004s for this model), t_{on} and t_{off} are the respective start and stop times of the torque activation (which are the parameters to be optimized), and n is used to smooth the activation and deactivation curve (1 for this model).

In addition to the active torque, there is a passive torque component to MTG, which serves as a restoring torque when the joint approaches the extremities of its ROM [14],[19],[20]. The formulation was developed by Yamaguchi and includes joint damping [14],[19],[20]. The equation is referenced in [14] and is written as follows:

$$T_{\text{passive}} = k_1 e^{-k_2(\theta-\theta_1)} - k_3 e^{-k_4(\theta_2-\theta)} - c_1\dot{\theta}$$

where the k-values are shape parameters, θ is the current joint angle, $\dot{\theta}$ is the current angular velocity, θ_1 and θ_2 are the joint angle breakpoints where the passive torque significantly increases (which can be viewed as the joint ROM bounds), and c_1 is a damping coefficient (0.1 in this model). The k-values and θ-values are shown in Table 3 for each joint. Note that the definition of joint coordinate system direction impacts the order of the k-values, which may differ from [14],[19],[20]. While the k-values came from [14],[19],[20], the θ values generally came from [21].

To generate the k-values, the passive torque equation was fit to experimental resistive torque measurements of the torso/pelvis, shoulder, elbow, and the wrist DOF movements with the exception of shoulder rotation [19],[20]. The data was

fit and plotted against joint angles. In order to generate the desired passive torque profile, four data points, that function as shape parameters, were generated using linear stiffness, and are the four k-values used in the passive equation [19],[20]. No experimental data was found for the passive torque of the trunk, so the pelvis' passive torque profile was also applied to the trunk [19],[20]. It is for this reason that the torque and pelvis are combined in this model, in addition to the fact that they both contribute to MAR/LAR. Furthermore, no data existed for shoulder rotation, so the approach outlined by Nasr was taken [21]. In the future, an experimental procedure should be done to identify the shape parameters for shoulder rotation.

TABLE III
PASSIVE TORQUE INPUT VARIABLES

Joint Movement	k_1	k_2	k_3	k_4	θ_1 (rad)	θ_2 (rad)
MAR/LAR	5.57	2.02	5.56	1.97	-0.868	0.868
H.FLX/EXT	4.3	1.65	7.03	2.31	-1.092	2.281
IR/ER	6	6	6	6	-1.521	2.967
E. FLX/EXT	3.55	20.6	0.39	7.85	0.093	2.344
W. FLX/EXT	1.74	2.01	1.01	2.03	-1.446	1.313

Most of the values inputted into the MTG equations were mostly sourced from [14],[19],[20], however, as briefly introduced, some changes were made to account for the extremely dynamic nature of the pitching motion, or if the required parameter was unavailable [14],[19-21]. This is discussed in the next subsection.

C. MTG Input Adjustment

The torque profiles of the MTG are shaped by the model inputs, many of which are human measures. If the human measures are taken from an average population, the expected torque profile will reflect that. Since these athletes have above average abilities, for example, in the maximum range of shoulder external rotation, the torque profiles must reflect that. As such, some MTG equation inputs were altered to reflect the superior muscular control, response time, flexibility and strength present in these athletes .

With justification from literature, a number of variables were changed. The activation and deactivation time constants were made much quicker and the shape factor (r) was decreased to increase the starting and ending slope of the torque profiles. In doing so, the MTG was able to reach full torque generation capabilities faster, which accounts for superior response times and increased muscular control of these athletes [21]. θ_1 and θ_2 for IR/ER were also increased since pitchers have extreme laxity in this DOF [3-11][21]. The maximum allowable torques and angular velocities were increased to account for the superior torque generating capabilities and strength of pitchers [11],[12]. Slight damping was also applied to the wrist and trunk MTG since the prescribed initial velocities caused nonphysical inertial responses for those segments, when subjected to the MTG.

With the model created and actuator behaviour defined, the model was exported as a Simulink (The MathWorks, Inc., MA, USA) block, so that simulations could be run in MATLAB (The MathWorks, Inc., MA, USA). MapleSim has a feature which allows conversion of a model into a Simulink block. In Simulink, the model becomes a black box containing all the kinematic, dynamic and constraint differential equation that can be accessed using MATLAB.

III. Optimization Formulation

A. Cost Function and Constraints

The aim of the optimization was to maximize the velocity of the end-effector, which is the hand-ball interface in the model, in the direction of the batter (positive x-direction). Note that the MATLAB optimization solvers minimize functions by default. As such, for maximization, the reciprocal of the function was minimized as follows:

$$J = max(|Velocity_x(t_{\text{final}})|) = min(\frac{1}{|Velocity_x(t_{\text{final}})|})$$

Although the cost function is very simple, it also produced the best results, compared to other potential costs. Some of the attempted functions included the absolute squared velocity, but since the optimization techniques used did not rely on derivatives/gradient calculations, this was unnecessary. Using the squared velocity also produced less accurate results, which is another reason why that cost function was abandoned. Another set of cost functions that were tested included a weighted absolute squared speed and weighted absolute speed, which considers all directions of speed (x, y, z). These attempted cost functions were set up to penalize velocity in the y and z-directions (non-batter directions). However, without a ball trajectory model as a parameter for the optimization, which could simulate the path of the ball based on the ball conditions at release, penalizing the throwing direction away from the batter was ineffective. As such, the weightings were abandoned. Even without weightings, considering all directions of speed produced impossible ball velocities, so that cost function was abandoned as well. Nonetheless, even while using the current cost, the y and z components of velocity were still measured and reported. By maximizing the velocity in the batter's direction, the results implied that there would be a reasonable forward progression of the ball, since the x-component should be the largest.

A crucial component of the cost function is the t_{final} term, which means that the velocity is measured at the terminating time of the simulation. To find the ideal time of simulation, literature was first consulted to get a rough estimate of the duration of the acceleration phase, which was between 0.042-0.058s [8],[17]. To determine the simulation time required, numerous iterations of the optimization were run with time steps that differed by 0.001 seconds. For a simulation duration that was too long, the MTG caused some highly nonphysical behaviours due to the initial conditions and passive torques correcting the model at the ends of the ranges of motion. For a short simulation, the error in the joint final positions compared to literature were far too high, since not enough time was allocated for the MTG to activate and move to their final position. The arm acceleration phase is one of the fastest and

most dynamic movements in sports and as such, the model was extremely sensitive to the duration of simulation. Ultimately, the best simulation outcomes were produced with a simulation time of 0.06 seconds.

Constraints were also an important component of the model and were checked against the simulation at each iteration. The key constraints in this model revolved around limits to human abilities in their joint ROM and torque generating capabilities. As such, each DOF was constrained to fall within reasonable human limits. Recall, however, that many values for torque and ROM were adjusted to account for an athlete's superior muscle control. It is also important to note that joint ROM is inherently constrained in the model, via θ_1 and θ_2 in the passive torque, which corrects the joint trajectory as it reaches the ends of its ROM. However, the inclusion of initial velocities meant that there was a possibility for the joint to go beyond the end ranges of its ROM, before the passive torque had a chance to activate and prevent this. As such, the ROM constraints had to be further enforced in the optimization as well and came from [21]. The athlete adjusted torques were also found from literature [3-6],[19],[20]. A combined max torque was also determined for the trunk and pelvis, since they both contribute to MAR/LAR [21].

ROM Constraints:

$$\textbf{-49.7}^\circ(LAR) \leq \theta_{\mathrm{MAR/LAR}} \leq \textbf{49.7}^\circ(MAR)$$

$$\textbf{-62.6}^\circ(H.EXT) \leq \theta_{\mathrm{H.FLX/EXT}} \leq \textbf{131.7}^\circ(H.FLX)$$

$$\textbf{-87.1}^\circ(IR) \leq \theta_{\mathrm{IR/ER}} \leq \textbf{170.0}^\circ(ER)$$

$$\textbf{-5.4}^\circ(E.EXT) \leq \theta_{\mathrm{E.FLX/EXT}} \leq \textbf{134.3}^\circ(E.FLX)$$

$$\textbf{-82.8}^\circ(W.FLX) \leq \theta_{\mathrm{W.FLX/EXT}} \leq \textbf{75.1}^\circ(W.EXT)$$

Torque Constraints:

$$\textbf{-450 Nm} \leq T_{\mathrm{MAR/LAR}} \leq \textbf{450 Nm}$$

$$\textbf{-160 Nm} \leq T_{\mathrm{H.FLX/EXT}} \leq \textbf{160 Nm}$$

$$\textbf{-160 Nm} \leq T_{\mathrm{IR/ER}} \leq \textbf{160 Nm}$$

$$\textbf{-90 Nm} \leq T_{\mathrm{E.FLX/EXT}} \leq \textbf{90 Nm}$$

$$\textbf{-60 Nm} \leq T_{\mathrm{W.FLX/EXT}} \leq \textbf{60 Nm}$$

An additional constraint check was put into place, to ensure that the MTG activation timing came before its respective deactivation timing. During each iteration, these constraints were checked, and if the constraints or timings were violated, the cost function would be penalized and return a significantly greater value than a constraint abiding iteration. This continued until the constraints were satisfied and the solver terminated.

B. Particle Swarm and Pattern Search Optimization

Particle swarm optimization was used to optimize the model. Particle swarm was selected due to its computational efficiency and ease of implementation [22]. Particle swarm also permits the use of a hybrid function, which will be discussed shortly.

The particle swarm optimization technique functions by creating a population of solutions (or particles) which move through a solution space in search of the minimum value at each iteration [22]. The particle movements are influenced by their known local minima but also the known solutions found by other particles [22]. The particle swarm optimization was conducted in MATLAB using the *particleswarm* function.

Once the particle swarm was complete, a hybrid function was implemented, which was the pattern search optimization technique. A hybrid function is a MATLAB optimization feature that continues the optimization after the original solver terminates [22]. In this case, it was used a second optimization method to obtain a more accurate solution, starting from the relatively rough solution found by the first solver [22]. It was ultimately implemented to ensure that both methods converged to an accurate global solution [22]. Once the particle swarm optimization terminated the built-in *patternsearch* function was automatically called. Pattern search optimization works by finding a sequence, or pattern, of points that approach an optimal point [22]. These two methods were selected because they are considered robust, are computationally efficient, easy to implement, and most importantly, do not require gradient or derivative calculations.

To reduce the CPU time, upper and lower limits were set for the torque timings. Numerous iterations with varying bounds were attempted, to ensure that a wide enough range was included, as to not miss any potentially viable solutions. If an outputted torque timing was along the boundary, the limit was increased, and the optimization was run again, until a viable solution was found.

After over 70 iterations and just over an hour of CPU time, both the particle swarm and pattern search methods terminated since the relative change in the objective value was less than the specified tolerance (0.00001). Both methods converged to the same solution, indicating a global solution was reached.

IV. Results

With the optimization complete, 14 torque timings, for the 7 MTG were outputted by the model, in addition to the optimized cost and ball speeds in each directions. The optimized torque timings are seen in Table 4, and the optimized simulation is visualized in Figure 3, where the optimized timing variables were inputted accordingly.

TABLE IV
OPTIMIZED TORQUE TIMINGS FOR A 60MS (0.06S) SIMULATION

DOF:	**MAR**	**H. FLX**	**IR**	**E. FLX**	**E. EXT**	**W. EXT**	**W. FLX**
t_{on} **(ms)**:	14.5	3.3	13.7	0	1.7	4.8	29
t_{off} **(ms)**:	50.9	60	49.1	0	36	11.1	39.6
Total:	36.4	59.67	35.4	0	34.3	6.3	10.6

Probes were also attached to the MapleSim model to measure joint angles. The joint angles were plotted against the time of simulation and compared against literature for validation and analysis.

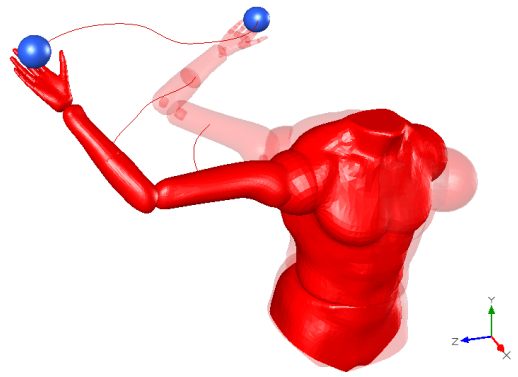

Fig. 3. Visualization of the initial (opaque) and final orientation of the model, using the optimized torque timings, in MapleSim. Tracers were included to highlight segment and ball trajectories.

The maximized ball velocity was 51.64 m/s, or 115.43 Mph, which is above the major league average of 93 Mph and fastest pitch ever recorded (105 Mph) [13]. However, the x-component was 35.51 m/s (79.43 Mph), while the y and z components were -14.83 and -34.45 m/s, respectively. Although the velocity in the direction of the batter was the largest, the z-component was also significant, which may indicate that this pitch would not reach the batter. However, this is not conclusive without a ball trajectory model.

V. Model Validation, Analyses and Discussion

To determine the validity of the model, first, the angular orientations of each joint at ball release (end of simulation) were compared to that of the literature, and are summarized in Table 4. Note that the angles correspond to the orientation depicted in Figure 3.

TABLE V
JOINT ANGLE COMPARISON AT BALL RELEASE [3],[6],[8],[17],[18],[23]

Joint	Literature Average	Simulation	Error
Elbow	63.3° EXT	51° EXT	12.3°
Shoulder (Horizontal)	13.6° H. FLX	11° H. EXT	24.6°
Shoulder (Rotational)	26.3° ER	34° ER	7.7°
Wrist	0° Neutral	9° FLX	9°
Trunk	14° MAR	4° MAR	10°

Considering the dynamic nature of a baseball pitch, the error between the joint angles at ball release in literature and simulation seem quite reasonable. Moreover, this model is highly simplified and does not consider the full body, or entire pitching motion. Another source of error may be that the published data sources are outdated or use old measurement and analyses techniques [17][23]. Considering these factors, the optimized model seems to have performed quite well. All joints had a relatively reasonable error, with the major outlier being the final position of the shoulder in the horizontal plane, where literature suggests that there should be slight flexion, while the model predicted some extension.

To further validate the optimized model's performance, joint angle trajectories that were available in literature were plotted and compared to those measured by the probes in the model. For fair comparison, both the time and angles were normalized as percentages of the maximum values. The plots are seen in Figures 4 and 5 and use data from Pappas et al [17] and Dillman et al [23].

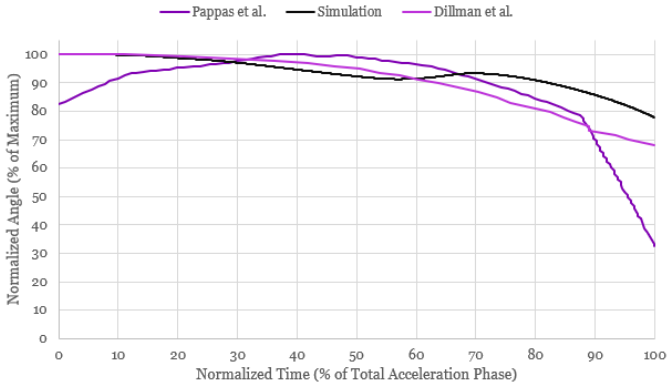

Fig. 4. Normalized shoulder ER (+)/IR(-) comparison between simulation and literature throughout the arm acceleration phase

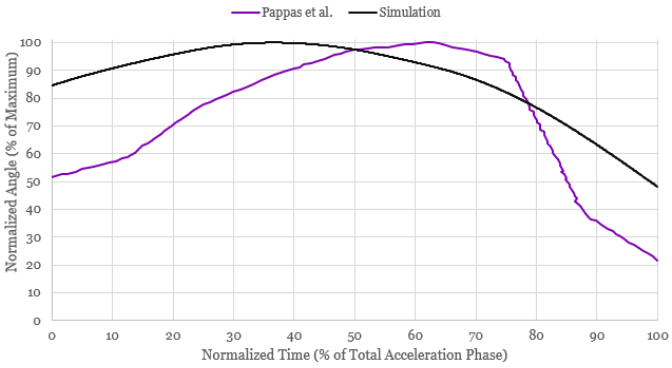

Fig. 5. Normalized elbow flexion (+)/extension(-) comparison between simulation and literature throughout the arm acceleration phase

Similar to the final joint angle error, the differences in trajectory seem quite reasonable, considering the dynamic nature of a baseball pitch. Further, since this model operates under many assumptions for simplicity and simulates only a fraction of time of the entire pitch, it is not surprising that discrepancies exist. Moreover, both pieces of literature that provided joint angles are over 30 years old, and one nearly 40 years old, implying that the data collection techniques may be outdated, putting the validity of the data into question [17][23]. Finally, both datasets also used very small sample sizes, of varying skill, which may have caused deviations, especially in the initial angles of the joints, which is reflected in Figures 4 and 5 [17][23].

Overall, when evaluating the differences between literature and this simulation, there are some key considerations that

should be made to justify such differences, a few of which have already been discussed. More notably, this model does not consider fatigue or any other factors that may limit human performance. It is very much an idealized model, and by optimizing an idealized model, it is no surprise that the model outperformed a real pitcher in generating velocity. This does not discount the results, rather, it demonstrates idealized pitching mechanics that can be used for educational purposes and to improve performance. The same can be said about the joint trajectory differences as well.

It is important to note some key observations relating to the optimized joint timings in Table 4 as well. It was determined that there should be no elbow flexion after peak shoulder external rotation is reached during the arm acceleration phase, which is reflected by the fact that the MTG never activates. This is confirmed to be accurate according to literature, since the elbow experiences a rapid rate of extension during arm acceleration [18]. Furthermore, it is observed that there is generally a sequential chain from the more proximal (trunk) to distal (hand/ball) segments, as reflected by the activation sequencing, which is also confirmed in literature [11]. Finally, it is seen that the trunk, elbow and more importantly the shoulder MTG, were activated for a majority of the simulation. This aligns with the literature that suggest that these 3 joints generate a majority of the pitching velocity in the upper body, which is consistent with their duration of activation [24]. Note that the upper body contributes to approximately 57.8% of total pitch velocity [24]. Contrary to the literature, there is a small instance of wrist extension, which seems negligible, but at no point should the wrist be extended in this phase [18]. This likely occurred due to the inertial properties of the ball, which caused the wrist to lag behind as the forward motion progressed, resulting in inadvertent wrist extension. To compensate for this, the optimization triggered wrist flexion, which is why the wrist ultimately ended up flexed, instead of neutral as literature suggests [17]. This will be addressed in future work, by adding more stiffness to the wrist's hinge joint, to reduce the effects of the ball's inertia on the hand.

A. Optimization Considerations

When considering the number of variables, constraints and complexity of the MapleSim model and associated Simulink block, the computational efficiency of the optimization was quite reasonable. An attempt was made to use alternative optimization techniques, such as the MATLAB interior point method, *fmincon*, which required more computational time and iterations, and did not accurately terminate or converge. This implies that the particle swarm and pattern search techniques had a fair computational efficiency.

As mentioned, the solution reached was a global one, since both techniques employed converged to the same results, and all timing, torque and ROM constraints were observed in the final solution. The satisfaction of constraints was also verified by simulating the optimized model in MapleSim, where it was confirmed that there were no constraint violations.

Since the optimization techniques used were not numerical methods, there was no sensitivity to initial guesses. Furthermore, considering the complexity and number of constraints, it is difficult to determine the exact feasible region. This also means that determining the modality of the function is difficult because the range is uncertain. However, since the simple cost of 1 over absolute value of x-velocity is used as the objective function, twice differentiating it indicates that all values of the that differentiated function would be greater than 0, for all inputs. This implies that the function is convex in nature, and that optimization would yield a minimum, which aligns with the expected results. Plotting the cost function also highlights that the function is strictly convex in two feasible areas, $x\epsilon[0,\infty]$ and $x\epsilon[0,-\infty]$, but without plotting the constraints, a visual global minimum in those ranges is hard to identify. The constraints were not plotted due to the number and complexity of the constraints, but the convergence of both solutions still implies a global solution was reached. Additionally, the function is nonunimodal in those ranges, even with the constraints, because the function is not strictly monotonic.

VI. Conclusions and Future Work

The aim of the project was to develop a multi DOF, 3D model of a pitcher's throwing arm and trunk, which will serve as the foundation for a more complex, full-body model in the future. Cumulative muscle forces were modelled as MTG, and the actuator firing times were optimized and reported to maximize velocity of the end-segment. Using the optimized times in simulation, predicted speeds and joint angles were measured and compared to literature. The comparisons were reasonable considering the model's assumptions, simplicity, idealized conditions and reliability of the data in the literature. The current findings are a good indication of proper pitching mechanics, which can be used to educate pitchers and improve their performance.

In the future, the first step would be to evaluate joint forces and torques of the model to assess injury risk under the optimized conditions. This would provide crucial insight into injury etiology of the throwing shoulder and elbow in pitchers, informing injury mitigation techniques. More work can be done to also understand how the differences in kinematics and physiology impact joint torques and soft tissue loads using this model. Next, building a full body model, with the complete DOF of the human anatomy, and simulating the entire duration of a pitch would be beneficial. This is no easy task but would allow for more definitive conclusions in comparison to literature. Moreover, it would be beneficial to compare the joint angle results from simulation to more modern and reliable data. The motion research group at the University of Waterloo has access to pitching data from high-level, professional players and is ready for kinematic analysis, but the data was not processed in time for this project. Finally, it would be beneficial to review and refine the MTG equation inputs, and more notably, collect and fit data to more accurately represent the passive torque profiles for shoulder and trunk rotation.

References

[1] B. Hansen, "Finite element analysis of the ulnar collateral ligament under various valgus loads," Motus Global Inc., Oct. 2019.

[2] D. P. Leland et al., "Prevalence of medial ulnar collateral ligament surgery in 6135 current professional baseball players: A 2018 update," Orthopaedic Journal of Sports Medicine, vol. 7, no. 9, Sep. 2019. doi:10.1177/2325967119871442.

[3] G. J. Calabrese, "Pitching Mechanics, Revisited," Int. J. Sports Phys. Th., vol. 8, no. 5, pp 652-660, 2013.

[4] M. E. Feltner and J. Dapena, "Three-Dimensional Interactions in a Two-Segment Kinetic Chain. Part I: General Model," Int. J. of Sp. Biom. (1989), vol. 5, no. 4, pp. 403-419, Mar. 2024, doi:10.1123/ijsb.5.4.403.

[5] K. Naito, T. Takagi, H. Kubota, and T. Maruyama, "Multi-body dynamic coupling mechanism for generating throwing arm velocity during baseball pitching," Hum. Mov. Sci., vol. 54, pp. 363–376, Aug. 2017, doi: 10.1016/j.humov.2017.05.013.

[6] D. F. Stodden, G. S. Fleisig, S. P. McLean, and J. R. Andrews, "Relationship of Biomechanical Factors to Baseball Pitching Velocity: Within Pitcher Variation," J. Appl. Biomech., vol. 21, no. 1, pp. 44-56, Feb. 2005, doi: 10.1123/jab.21.1.44.

[7] G. Fleisig, "Biomechanics of Baseball Pitching: Implications for Injury and Performance," Int. Symp. Biomech. in Sports, vol. 28, Jul. 2010.

[8] A. Z. Diffendaffer et al., "The Clinician's Guide to Baseball Pitching Biomechanics," Sports Health, vol. 15, no. 2. SAGE Publications Inc., pp. 274–281, Mar. 01, 2023. doi: 10.1177/19417381221078537.

[9] A. L. Aguinaldo and H. Chambers, "Correlation of throwing mechanics with elbow valgus load in adult baseball pitchers," American Journal of Sports Medicine, vol. 37, no. 10, pp. 2043–2048, 2009, doi: 10.1177/0363546509336721.

[10] T. P. Torabi, B. Juul-Kristensen, M. Dam, M. K. Zebis, R. van den Tillaar, and J. Bencke, "Comparison of throwing kinematics and muscle activation of female elite handball players with and without pain–the effect of repeated maximal throws," Sports Biomechanics, 2023, doi: 10.1080/14763141.2023.2212645.

[11] R. McN. Alexander, "Optimum timing of muscle activation for simple models of throwing," Journal of Theoretical Biology, vol. 150, no. 3, pp. 349–372, Jun. 1991,doi:10.1016/s0022-5193(05)80434-5.

[12] T. Matsuo, T. Matsumoto, Y. Mochizuki, Y. Takada, and K. Saito, "Optimal shoulder abduction angles during baseball pitching from maximal wrist velocity and minimal kinetics viewpoints," J. Appl. Biomech., vol. 18, no. 4, pp. 306–320, Nov. 2002. doi:10.1123/jab.18.4.306.

[13] N. Fujii and M. Hubbard, "Validation of a three-dimensional baseball pitching model," J. Appl. Biomech., vol. 18, no. 2, pp. 135–154, May 2002. doi:10.1123/jab.18.2.135.

[14] W. McNally and J. McPhee, "Dynamic Optimization of the Golf Swing Using a Six Degree-of-Freedom Biomechanical Model," MDPI AG, Feb. 2018, p. 243. doi:10.3390/proceedings2060243.

[15] P. de Leva, "Adjustments to Zatsiorsky-Seluyanov's segment inertia parameters," Journal of biomechanics, vol. 29, no. 9, pp. 1223-30, 1996 doi:10.1016/0021-9290(95)00178-6.

[16] E. Goleckyte, "Baseball size and dimensions - size-charts.com - when size matters," Size Charts, https://size-charts.com/topics/sports-size-chart/baseball-size-and-dimensions/(accessed Apr. 4, 2024).

[17] A. M. Pappas, R. M. Zawacki, and T. J. Sullivan, "Biomechanics of baseball pitching A preliminary report," Am. J. Sports. Med., vol.13, no. 4, pp. 216-222, 1985, doi:10.1177/036354658501300402.

[18] Y. Kaizu, E. Sato, and T. Yamaji, "Biomechanical analysis of the pitching characteristics of adult amateur baseball pitchers throwing standard and lightweight balls," J Phys. Ther. Sci., vol. 32, pp. 816-822, 2020.

[19] W. McNally, "Forward dynamic simulation of a Golf Drive: Optimization of golfer biomechanics and equipment," MASc thesis, Dept. Systems Design Engineering, University of Waterloo, Waterloo, ON, Canada, 2018.

[20] S. Ferguson, "A Two-Armed Forward Dynamic Model of a Golf Drive: A Simulation and Optimization Tool for Golf Equipment and Biomechanics," MASc thesis, Dept. Systems Design Engineering, University of Waterloo, Waterloo, ON, Canada, 2023.

[21] A. Nasr, A. Hashemi, and J. McPhee, "Scalable musculoskeletal model for dynamic simulations of upper body movement," Computational Methods Biomechanical and Biomedical Engineering, 2023, doi: 10.1080/10255842.2023.2184747.

[22] M. R. Bonyadi and Z. Michalewicz, "Particle swarm optimization for single objective continuous space problems: A Review," Evolutionary Computation, vol. 25, no. 1, pp. 1–54, 2017.

[23] C. J. Dillman, G. S. Fleisig, and J. R. Andrews, "Biomechanics of pitching with emphasis upon shoulder kinematics," Journal of Orthopaedic and Sports Physical Therapy, vol. 18, no. 2, pp. 402–408, Aug. 1993. doi:10.2519/jospt.1993.18.2.402.

[24] G. J. Alderink, T. Kepple, S. J. Stanhope, and A. Aguinaldo, "Upper body contributions to pitched ball velocity in elite high school pitchers using an induced velocity analysis," Journal of Biomechanics, vol. 120, p. 110-117, May 2021. doi:10.1016/j.jbiomech.2021.110360.